

Testing the standard model versus left-right models on and off the Z resonance

V. Barger

*Department of Physics, University of Durham, Durham City DH1 3LE, England
and Department of Physics, University of Wisconsin, Madison, Wisconsin 53706*

Ernest Ma

Department of Physics and Astronomy, University of Hawaii, Honolulu, Hawaii 96822

K. Whisnant

Department of Physics and Ames Laboratory, Iowa State University, Ames, Iowa 50011

(Received 7 March 1983)

We examine the high-energy predictions of left-right models which are consistent with constraints from low-energy data. These are compared to the predictions of the standard electroweak gauge model to determine how well the theories can be distinguished by measurements in this mass region of the standard Z boson resonance. We find a nontrivial class of left-right models in which the lowest-mass Z is indistinguishable in mass and fermion couplings from the standard Z , but which allow a second Z boson as low as 200 GeV. We discuss the sensitivity of the lower limit on the second- Z mass to the results of the atomic parity-violation measurement and find that the newest data relaxes the mass limit in a general left-right model to $M_{Z_2} \geq 150$ GeV.

I. INTRODUCTION

In the next few years, experiments at e^+e^- and $\bar{p}p$ colliders will provide much additional information about the structure of the electroweak interactions. The standard electroweak gauge model¹ is consistent with all low-energy phenomena,² but there are alternative models with additional neutral currents which also describe existing data. How well will the next round of experiments at higher-energy machines be able to differentiate the competing theories? For the case of left-right models, we will show that while a large number of models can be distinguished, there exists a nontrivial class of solutions which cannot be ruled out by forthcoming experiments even if a "standard" Z boson is discovered.

Previously we have derived the most general electroweak interaction with two neutral currents in a theory free of triangle anomalies.³ For the special case of left-right models with gauge group $SU(2)_L \times SU(2)_R \times U(1)_{B-L}$ (Refs. 4–9) or $SU(2)_L \times U(1)_R \times U(1)_{B-L}$ (Refs. 10–15) we found restrictions on the parameters of the theory from existing neutral-current data. In this paper, we will examine the high-energy predictions of left-right models consistent with those constraints and compare them with the standard-model results.

In Sec. II we examine how well left-right models can be differentiated from the standard model in experiments at center-of-mass energies in the range 50–120 GeV. We find that measurements off the Z resonance are unlikely to provide significant constraints on left-right models, beyond those obtained from low-energy data. However, measurements on the Z resonance will greatly reduce the allowed range of parameters in a general left-right model.

The standard electroweak gauge model is characterized

by one mixing angle. Should measurements on the Z resonance not be consistent with this single parameter, then one must turn to an alternative model. On the other hand, if the Z resonance is identical in all respects to the single Z of the standard model, are alternative models necessarily ruled out? In alternative models of the type $SU(2) \times U(1) \times G$ where the fermions are neutral under G ,^{16–22} a Z_1 which is identical to the standard Z implies the theory must approach its standard model limit at all energies. However, left-right models are not so limited. In Sec. III, we discuss a class of left-right models in which the lowest-mass Z boson is indistinguishable from the standard Z and which yet allow a second Z with a mass as low as 200 GeV. This situation occurs when the Z_1 - Z_2 mass matrix is diagonal, or nearly so. The fermions still couple to the Z_2 with a mixture of left-handed, right-handed, and electromagnetic currents. This differs from a standard-model limit in that the fermion couplings to the Z_2 are not artificially small. Since differentiation from the standard model may be impossible near the Z_1 for this class of models, we examine the likelihood of direct detection of the Z_2 in $\bar{p}p$ colliders and find that there is the possibility that it can be detected at the proposed Fermilab Tevatron.

Finally, in Sec. IV we discuss the data used to constrain the parameters of the low-energy neutral-current Hamiltonian in left-right models. The analysis uses the same data as the standard-model analysis of Kim *et al.*,²³ except that the latest e^+e^- annihilation and atomic parity-violation data are included. We find that the lower limit on the Z_2 mass is particularly sensitive to the atomic parity-violation measurement and that the most recent data²⁴ are less restrictive than previous results. The revised Z_2 mass limit for a general left-right model is $M_{Z_2} \geq 150$ GeV at the 1σ level.

II. LEFT-RIGHT-MODEL PREDICTIONS NEAR THE Z_1 RESONANCE

In this section we examine the high-energy predictions of left-right models whose parameters are constrained by fits to low-energy data. We concentrate our attention on observables measurable in e^+e^- annihilation at $\sqrt{s} \geq 50$ GeV and at $\bar{p}p$ colliders. We compare the results with the predictions of the standard model to determine how well left-right models can be differentiated from the standard model.

The neutral-current interaction for a general left-right model is

$$\mathcal{H} = g_L W_{3L} J_{3L} + g_R W_{3R} J_{3R} + \frac{1}{2} g_C C J_{B-L}. \quad (1)$$

The neutral gauge bosons W_{3L} , W_{3R} , and C can be rotated to a new basis consisting of the photon A , the usual neutral gauge field Z , and an additional field D by the transformation

$$\begin{aligned} W_{3L} &= x_L^{1/2} A + (1-x_L)^{1/2} Z, \\ W_{3R} &= x_R^{1/2} A - (x_L x_R)^{1/2} (1-x_L)^{-1/2} Z \\ &\quad + (1-x_L-x_R)^{1/2} (1-x_L)^{-1/2} D, \\ C &= (1-x_L-x_R)^{1/2} A \\ &\quad - (1-x_L-x_R)^{1/2} x_L^{1/2} (1-x_L)^{-1/2} Z \\ &\quad - x_R^{1/2} (1-x_L)^{-1/2} D, \end{aligned} \quad (2)$$

where $x_L = e^2/g_L^2$, $x_R = e^2/g_R^2$, and the electric charge e is given by $e^{-2} = g_L^{-2} + g_R^{-2} + g_C^{-2}$. Then Eq. (1) becomes

$$\mathcal{H} = g_Z Z J_{ZL} + g_Z D [\beta J_{ZL} + (\alpha + \beta) J_{ZR}], \quad (3)$$

where we have defined $J_{ZL} = J_{3L} - x_L J_{EM}$, $J_{ZR} = J_{3R} - x_R J_{EM}$, $g_Z = e x_L^{-1/2} (1-x_L)^{-1/2}$, and

$$\beta = (x_L x_R)^{1/2} (1-x_L-x_R)^{-1/2}, \quad (4a)$$

$$\alpha + \beta = (1-x_L) x_L^{1/2} (1-x_L-x_R)^{-1/2} x_R^{-1/2}. \quad (4b)$$

Given the most general mass-squared matrix for the Z and D gauge bosons

$$\mathcal{M}^2 = g_Z^2 \begin{pmatrix} A & B \\ B & C \end{pmatrix}, \quad (5)$$

the effective low-energy neutral-current interaction is

$$\mathcal{H}^{\text{eff}} = \frac{4G_F}{\sqrt{2}} [(\rho_1 J_{ZL})^2 + (\rho_2 J_{ZL} + \eta J_{ZR})^2], \quad (6)$$

with

$$\frac{8G_F}{\sqrt{2}} \rho_1^2 = A^{-1}, \quad (7a)$$

$$\rho_2/\rho_1 = (\beta - B/A)/(C/A - B^2/A^2)^{1/2}, \quad (7b)$$

$$\eta/\rho_1 = (\alpha + \beta)/(C/A - B^2/A^2)^{1/2}. \quad (7c)$$

Only the relative signs of ρ_2 and η is physically relevant; we will choose the convention $\rho_2 \geq 0$. The precise neutral-current Hamiltonian in the mass-eigenstate basis

(Z_1, Z_2) may be found by diagonalizing \mathcal{M}^2 . For the rotation matrix

$$R = \begin{pmatrix} \cos\psi & -\sin\psi \\ \sin\psi & \cos\psi \end{pmatrix}. \quad (8)$$

$R \mathcal{M}^2 R^{-1}$ is diagonal when

$$\tan 2\psi = 2B/(C-A). \quad (9)$$

Requiring $M_{Z_1} < M_{Z_2}$ implies

$$2B \sin 2\psi > (A-C) \cos 2\psi. \quad (10)$$

The neutral-current interaction of Eq. (3) can now be written

$$\mathcal{H} = g_Z \sum_{i=1}^2 \left[\sum_f \bar{f} \gamma_\mu (g_V^f + g_A^f \gamma_5) f \right] Z_i, \quad (11)$$

where

$$\begin{aligned} g_V^1 &= (\cos\psi - \beta \sin\psi) (\frac{1}{2} I_3 - Q x_L) \\ &\quad - (\alpha + \beta) \sin\psi (\frac{1}{2} I_3 - Q x_R), \end{aligned} \quad (12a)$$

$$\begin{aligned} g_V^2 &= (\sin\psi + \beta \cos\psi) (\frac{1}{2} I_3 - Q x_L) \\ &\quad + (\alpha + \beta) \cos\psi (\frac{1}{2} I_3 - Q x_R), \end{aligned} \quad (12b)$$

$$g_A^1 = -(\cos\psi + \alpha \sin\psi) \frac{1}{2} I_3, \quad (12c)$$

$$g_A^2 = -(\sin\psi - \alpha \cos\psi) \frac{1}{2} I_3. \quad (12d)$$

The allowed regions of x_L , x_R , ρ_1 , ρ_2 , and η consistent with low-energy neutral-current data have already been determined from data that were available a year ago³; we update that analysis using more recent measurements. The standard model limit is $\eta = 0$ and either $\rho_1 = 1, \rho_2 = 0$ or $\rho_1 = 0, \rho_2 = 1$. A useful alternative set of parameters is x_L , x_R , M_{Z_1} , M_{Z_2} , and ψ . The standard-model limit is then $\psi \rightarrow 0$, $M_{Z_2} \rightarrow \infty$, and x_L determined by $M_{Z_1} = M_W (1-x_L)^{-1/2}$.

A. $e^+e^- \rightarrow l^+l^-$ off resonance

High-energy e^+e^- annihilation into lepton pairs provides the cleanest probe of weak-interaction effects. The interference of weak and electromagnetic processes are very sensitive to the weak coupling parameters at center-of-mass energies near the neutral-gauge-boson masses. We will examine the reactions $e^+e^- \rightarrow \mu^+\mu^-$ and $e^+e^- \rightarrow \tau^+\tau^-$ in which only s -channel contributions are present. The principal measurements are the total cross section, angular asymmetries, and polarization effects; the latter can be determined by using initial-beam polarization or by measuring the helicity of a final-state lepton. A fit to the shape of these measurements versus center-of-mass energy \sqrt{s} would in principle greatly aid the determination of the weak parameters in the general left-right model.

We focus attention here on well-defined features of the measurements given above: positions and magnitudes of extrema, zeroes, and slopes. Consideration of measurements on resonance are deferred to the next section. We

will always assume e - μ - τ universality; more general formulas are available in the literature.²⁵

We first write down the differential cross section into μ or τ pairs, with helicity h of the negative final-state lepton, for an arbitrary number of Z bosons; in terms of $z = \cos\theta$

$$\frac{d\sigma}{dz} = \frac{\pi\alpha^2}{4s} [(1+z^2)(F_1 + hF_3) + 2z(F_2 + hF_3)], \quad (13)$$

where

$$F_1 = 1 + 2 \sum_j g_{Vj}^2 \chi_j + \sum_{j,k} (\chi_j \chi_k + \eta_j \eta_k) (g_{Vj} g_{Vk} + g_{Aj} g_{Ak})^2, \quad (14a)$$

$$F_2 = 2 \sum_j g_{Aj}^2 \chi_j + \sum_{j,k} (\chi_j \chi_k + \eta_j \eta_k) (g_{Vj} g_{Ak} + g_{Aj} g_{Vk})^2, \quad (14b)$$

$$F_3 = \sum_j 2g_{Vj} g_{Aj} \chi_j + \sum_{j,k} (\chi_j \chi_k + \eta_j \eta_k) 2g_{Vj} g_{Aj} (g_{Vk}^2 + g_{Ak}^2), \quad (14c)$$

and

$$\chi_j \equiv x_L^{-1} (1-x_L)^{-1} s (s - M_{Z_j}^2) \times [(s - M_{Z_j}^2)^2 + M_{Z_j}^2 \Gamma_{Z_j}^2]^{-1}, \quad (15a)$$

$$\eta_j \equiv -x_L^{-1} (1-x_L)^{-1} s M_{Z_j} \Gamma_{Z_j} \times [(s - M_{Z_j}^2)^2 + M_{Z_j}^2 \Gamma_{Z_j}^2]^{-1}. \quad (15b)$$

If instead the helicity of the final-state antilepton is measured, the F_3 terms in Eq. (13) have the opposite sign. The η_j contributions are relatively small for $|\sqrt{s} - M_{Z_j}| > \Gamma_{Z_j}$ and are ignored below whenever possible.

The maxima, minima, and zeros for the total cross section and asymmetry have been discussed previously for the case of the standard Z boson.²⁶ In left-right models, $M_{Z_2} \gtrsim 2M_Z$, so that it is plausible that one- Z formulas with Z_1 parameters will approximate the exact two- Z results in the vicinity of the Z_1 resonance or at energies below it. We find that such an approximation is good to an accuracy of 8%. In Fig. 1 we show the allowed regions of g_{V1} and g_{A1} for charged leptons in left-right models within 68% confidence limits. These quantities and the mass M_{Z_1} essentially determine the behavior for $\sqrt{s} \lesssim M_{Z_1}$.

The total cross section for $e^+e^- \rightarrow l^+l^-$ ($l = \mu, \tau$), normalized to the pointlike QED cross section, is

$$R^l = \sigma(e^+e^- \rightarrow l^+l^-) / \sigma(e^+e^- \rightarrow \gamma \rightarrow l^+l^-) = F_1. \quad (16)$$

For a single Z , the ratio R^l has a minimum value of

$$R_{\min}^l = 1 - g_V^4 / (g_V^2 + g_A^2)^2 \quad (17)$$

at

$$\sqrt{s} = m_Z / \{1 + (g_V^2 + g_A^2)^2 / [g_V^2 x_L (1-x_L)]\}^{1/2}. \quad (18)$$

Because $(g_{V1}/g_{A1})^2$ is small, the deviation of the minimum below unity is negligible.

The integrated forward-backward asymmetry is given by

$$A^{\text{FB}} = \frac{\int_0^{\pi/2} d\sigma - \int_{\pi/2}^{\pi} d\sigma}{\int_0^{\pi/2} d\sigma + \int_{\pi/2}^{\pi} d\sigma} = \frac{3}{4} \frac{F_2}{F_1}. \quad (19)$$

For one Z boson, the minimum value for A^{FB} is

$$A_{\min}^{\text{FB}} = \frac{3}{4} g_A^2 (g_A^2 + 2g_V^2)^{-1}, \quad (20)$$

which occurs at

$$(s_{\min})^{1/2} = M_Z / [1 + (3g_V^2 + g_A^2) x_L^{-1} (1-x_L)^{-1}]^{1/2}. \quad (21)$$

The maximum value is

$$A_{\max}^{\text{FB}} = \frac{3}{4} \quad (22)$$

and occurs at

$$(s_{\max})^{1/2} = M_Z / [1 - (g_V^2 - g_A^2) x_L^{-1} (1-x_L)^{-1}]^{1/2}. \quad (23)$$

Also $A^{\text{FB}} = 0$ at c.m. energy

$$(s_0)^{1/2} = M_Z / [1 + 2g_V^2 x_L^{-1} (1-x_L)^{-1}]^{1/2}. \quad (24)$$

Table I shows the deviation from the standard-model values for the observables in Eqs. (20)–(24). In each case the left-right model has been compared to the standard model with $M_{Z_1} = M_Z$. Also shown is a typical expected experimental error for each quantity. The expected fractional error of the A^{FB} measurements is about 15–20% near $(s_{\min})^{1/2}$ and 10–15% near $(s_{\max})^{1/2}$.²⁷ A fit to several points nearest each extreme may reduce this error by one-half. We estimate the positions of the extrema to have a fractional error of roughly one-third that of one

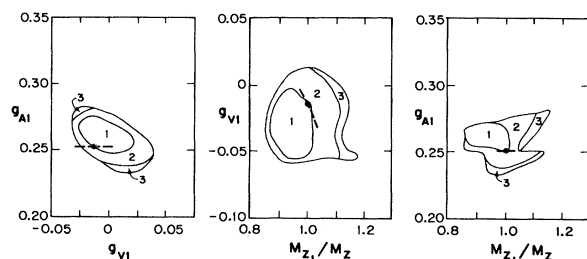


FIG. 1. Allowed ranges of charged-lepton couplings g_{V1} and g_{A1} in left-right models. The mass M_{Z_1} is specified relative to the standard-model mass M_Z at $x_W = 0.233$. Subregions are labeled according to the lowest realizable Z_2 mass: (1) $M_{Z_2}/M_Z < 2$, (2) $2 \leq M_{Z_2}/M_Z < 5$, and (3) $5 \leq M_{Z_2}/M_Z < 10$ (larger values of M_{Z_2} are also possible). The dashed lines are the standard-model predictions for x_W ranging from 0.215 to 0.251. The solid point represents the standard-model result for $x_W = 0.233$.

TABLE I. Maximal deviation of the off-resonance predictions for left-right models allowed by low-energy neutral-current data from those of the standard model. A given left-right model is compared to the standard model with a Z mass equal to M_{Z_1} . Also shown is the expected experimental uncertainty for each measurement.

	Standard model ($x_W=0.233$)	Maximal left-right-model deviation	Expected experimental uncertainty
A_{\min}^{FB}	-0.74	± 0.09	0.08
$(s_{\min})^{1/2}$	75 GeV	± 3 GeV	3 GeV
A_{\max}^{FB}	0.75	-0.18	0.05
$(s_{\max})^{1/2}$	110 GeV	± 7 GeV	4 GeV
$(s_0)^{1/2}$	89 GeV	+1.5 GeV	0.2 GeV

A^{FB} measurement, from the curvature of A^{FB} in those regions. The only observable which can significantly deviate from the standard-model predictions is A_{\max}^{FB} . Unfortunately, radiative corrections are most severe in this energy range, affecting A^{FB} by as much as a factor of 4.²⁸ The other potentially useful measurement is $(s_0)^{1/2}$. However, its precision is due to its closeness to resonance and adds no information that is not learned from the resonance measurements discussed in the next section. Unless the measurement uncertainties for the quantities in Table I are significantly better than the error values quoted there, left-right models cannot be clearly distinguished from the standard model away from the Z_1 resonance even at center-of-mass energies near 100 GeV.

The angle-averaged polarization of the final state lepton l^- is

$$P_l = \frac{\sigma(h=1) - \sigma(h=-1)}{\sigma(h=1) + \sigma(h=-1)} = \frac{F_3}{F_1} \quad (25)$$

for unpolarized beams when $e\text{-}\mu\text{-}\tau$ universality is assumed. The corresponding expression for longitudinal polarization $\pm P_e$ of the electron beam and unpolarized final states is identical to Eq. (25), except for an additional factor of P_e multiplying F_3/F_1 . Expected rates for initial or final polarization experiments are a factor 15–30 times less than unpolarized rates. Therefore, we shall discuss polarization measurements only in the resonance region where rates are enhanced.

B. $e^+e^- \rightarrow l^+l^-$ on the Z_1 resonance

Measurements at a Z pole in $e^+e^- \rightarrow l^+l^-$ provide a means of determining the vector and axial vector couplings of that Z to the charged leptons. Since left-right models have the bounds $83 \text{ GeV} < M_{Z_1} < 116 \text{ GeV}$, the Z_1 in these models should be accessible for study at either SLC or LEP. The initial data on the Z_1 will be its mass and width. The mass measurement should increase the precision of x_W in the standard model by a factor of 10, so that for practical purposes, it becomes a known quantity. Radiative corrections to the Z mass²⁹ must be taken into account in the x_W determination. For a given Z_1 mass, x_L can vary no more than about 0.005 from x_W and still be consistent with constraints from low-energy data.

The width of a Z in left-right models with massless fermions is

$$\Gamma_{Z_i} = g_{Z_i}^2 M_{Z_i} \sum_f c_f [(g_{V_i}^f)^2 + (g_{A_i}^f)^2] / 12\pi, \quad (26)$$

where c_f is the color factor ($c_f=3$ for quarks and $c_f=1$ for leptons). QCD corrections raise the hadronic width by about 4%.³⁰ For $m_t=25$ GeV the t -quark contribution is about 25% below the value for a massless quark. Using the couplings from the low-energy data analysis, we find that Γ_{Z_1} can vary by as much as 10% from the standard-model prediction for the same Z mass. The variation is comparable to the 6% contribution of a single neutrino species. Thus, measuring the Z width is not an unambiguous means of counting neutrinos, and emphasizes the need for a more direct neutrino measurement, such as $e^+e^- \rightarrow \gamma Z \rightarrow \gamma \nu \bar{\nu}$ above resonance.³¹ Branching ratios for $Z_1 \rightarrow l^+l^-, \bar{\nu}\nu, q\bar{q}$ can vary by 0.5%, 1%, and 2%, respectively, from their standard-model values.

The normalized total cross section for $e^+e^- \rightarrow l^+l^-$ on resonance is

$$R^l(\sqrt{s}=M_{Z_1}) = (M_{Z_1}/\Gamma_{Z_1})^2 (g_{V_1}^2 + g_{A_1}^2) [x_L(1-x_L)]^{-2}. \quad (27)$$

When combined with the forward-backward asymmetry,

$$A^{\text{FB}}(\sqrt{s}=M_{Z_1}) = \frac{3}{4} \left[\frac{2g_{V_1}g_{A_1}}{g_{V_1}^2 + g_{A_1}^2} \right]^2, \quad (28)$$

the magnitudes of the couplings can be deduced, modulo the factor $x_L(1-x_L)$. The relative sign of g_{V_1} and g_{A_1} can then be determined from the net final state polarization of the produced lepton

$$P^l(\sqrt{s}=M_{Z_1}) = \frac{2g_{V_1}g_{A_1}}{g_{V_1}^2 + g_{A_1}^2}. \quad (29)$$

The couplings g_{V_1} and g_{A_1} for charged leptons are given by Eq. (12) with $I_3 = -\frac{1}{2}$ and $Q = -1$. Figure 2 shows the allowed ranges of these resonance measurements versus Z_1 mass. The solid point is the standard-model prediction for x_W at its best-fit value of 0.233 and the dashed curve represents the presently allowed standard-model values in the range $x_W=0.215$ to 0.251 (2σ).

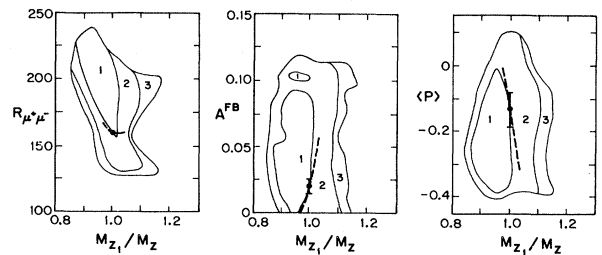


FIG. 2. Allowed ranges of on-resonance values at $\sqrt{s}=M_{Z_1}$ of R , A^{FB} , and $\langle P_l^- \rangle$ in $e^+e^- \rightarrow \mu^+\mu^-$ versus M_{Z_1}/M_Z . The error bars indicate estimated uncertainties for e^+e^- collider experiments. Notation as in Fig. 1.

Ranges of the minimum allowed Z_2 mass values are represented by the three numbered regions in the figure (see caption). Region 3 in Fig. 2 corresponds to models in which the fermion couplings to the Z_2 are large; hence M_{Z_2} cannot be too low. We note that measurements in agreement with the standard model would still allow left-right models with a relatively low Z_2 mass. This possibility is examined in detail in Sec. III.

Another measurement which may be possible is the slope of the forward-backward asymmetry in the region of the Z resonance. While the value of A^{FB} on resonance depends only on the Z_1 couplings to the fermions, the slope on resonance is affected by the Z_2 . In calculating the slope from Eqs. (14) and (19), the η_j terms must be kept. To leading order in $\Gamma_{Z_1}^{-2}$ the logarithmic derivative $D(\sqrt{s}) \equiv s dA^{\text{FB}}/ds$ evaluated at $s = M_{Z_1}^2$ is

$$D(M_{Z_1}) = \frac{3}{2}(g_{V1}^2 + g_{A1}^2)^{-4} \{ g_{A1}^2(g_{A1}^2 - g_{V1}^2)(3g_{V1}^2 + g_{A1}^2)x_L(1-x_L) - M_{Z_1}^2(M_{Z_2}^2 - M_{Z_1}^2)^{-1} [(g_{V1}^2 + g_{A1}^2)^2(g_{V1}g_{A2} + g_{A1}g_{V2})^2 - 4g_{V1}^2g_{A1}^2(g_{V1}g_{V2} + g_{A1}g_{A2})^2] \}, \quad (30)$$

which expanded in powers of $\epsilon = g_{V1}/g_{A1}$ is related to the value $D(M_{Z_1}; g_{V2} = g_{A2} = 0) \equiv D_1(M_{Z_1})$ by

$$D(M_{Z_1}) \simeq D_1(M_{Z_1}) [1 - M_{Z_1}^2(M_{Z_2}^2 - M_{Z_1}^2)^{-1}(g_{V2}^2 + 2\epsilon g_{V2}g_{A2} - 3\epsilon^2 g_{A2}^2)x_L^{-1}(1-x_L)^{-1}]. \quad (31)$$

For example, with $g_{V2} = \frac{1}{4}$, $x_L = 0.232$, and $M_{Z_2} = 2M_{Z_1}$ there is a 12% change from the one- Z result, i.e., $D_1(M_{Z_1})$. If a scan across the Z_1 can achieve a ± 0.05 error in A^{FB} at the peak, the error in $s dA^{\text{FB}}/ds$ may be of order 5%. Figure 3 shows the allowed range of $s dA^{\text{FB}}/ds$ versus Z_1 mass. Comparing Table I with Figs. 2 and 3, we see that measurements on the Z_1 resonance provide much better discrimination among models than measurements off resonance and would greatly reduce the allowed parameter region of left-right models.

C. $\bar{p}p \rightarrow l^+l^-X$ on the Z_1 Resonance

The Z boson can be produced in hadron collisions via quark-antiquark annihilation and observed through its decay into muon pairs. The cross section for the subprocess $\bar{q}q \rightarrow \mu^+\mu^-$ in any two- Z model can be written as

$$\frac{d\sigma^{\bar{q}q}}{d\cos\theta^*} = \frac{\pi\alpha^2 Q_q^2}{4m^2} [(1 + \cos^2\theta^*)(G_1^q + hG_3^q) + 2\cos\theta^*(G_2^q + hG_4^q)], \quad (32)$$

where θ^* is the angle of the outgoing l^- with respect to the p beam in the $\bar{q}q$ center of mass, m is the lepton-pair mass, h is the helicity of the l^- , and

$$G_1^q = 1 - \frac{2}{Q_q} \sum_j \chi_j g_{Vj}^q g_{Vj}^q + \frac{1}{Q_q^2} \sum_{j,k} (\chi_j \chi_k + \eta_j \eta_k) (g_{Vj}^q g_{Vk}^q + g_{Aj}^q g_{Ak}^q) (g_{Vj}^q g_{Vk}^q + g_{Aj}^q g_{Ak}^q), \quad (33a)$$

$$G_2^q = -\frac{2}{Q_q} \sum_j \chi_j g_{Aj}^q g_{Aj}^q + \frac{1}{Q_q^2} \sum_{j,k} (\chi_j \chi_k + \eta_j \eta_k) (2g_{Vj}^q g_{Ak}^q) (g_{Vj}^q g_{Ak}^q + g_{Aj}^q g_{Vk}^q), \quad (33b)$$

$$G_3^q = -\frac{2}{Q_q} \sum_j \chi_j g_{Vj}^q g_{Aj}^q + \frac{1}{Q_q^2} \sum_{j,k} (\chi_j \chi_k + \eta_j \eta_k) (2g_{Vj}^q g_{Ak}^q) (g_{Vj}^q g_{Vk}^q + g_{Aj}^q g_{Ak}^q). \quad (33c)$$

G_4^q is found from G_3^q by the interchange of μ and q superscripts on the couplings. In the above Q_q is the quark charge and χ_j and η_j are given by Eq. (15) with s replaced by m^2 . The $\bar{p}p$ cross section is found by folding in the momentum distribution of the initial quarks in the hadrons

$$\frac{d\sigma}{dy dm d\cos\theta^*} = \frac{2x_+ x_-}{3m} \sum_q f_q^p(x_+, m^2) f_q^{\bar{p}}(x_-, m^2) \frac{d\sigma^{\bar{q}q}}{d\cos\theta^*}. \quad (34)$$

The summation is over all quark and antiquark flavors and y is the rapidity of the lepton pair, with $x_{\pm} = m \exp(\pm y)/\sqrt{s}$. The angle θ^* is related to the corresponding laboratory angle θ by

$$\cos\theta^* = \frac{\cos\theta(x_+ + x_-) - (x_- - x_+)}{(x_+ + x_-) - (x_- - x_+)\cos\theta}. \quad (35)$$

Thus, the separation between forward and backward directions in the laboratory frame occurs at

$$\cos\theta^*(\theta = 90^\circ) = -(x_- - x_+) / (x_+ + x_-) = 1 - 2/(1 + e^{2y}). \quad (36)$$

On the Z_1 resonance the angular integration over forward and backward hemispheres in the laboratory frame can be done analytically to yield the forward-backward asymmetry

$$A^{\text{FB}}(m = M_{Z_1}) = \frac{2g_{V1}^q g_{A1}^q}{(g_{V1}^q)^2 + (g_{A1}^q)^2} \frac{\sum_q 2g_{V1}^q g_{A1}^q (H^q - 2H_1^q)}{\sum_q [(g_{V1}^q)^2 + (g_{A1}^q)^2] H_1^q}, \quad (37)$$

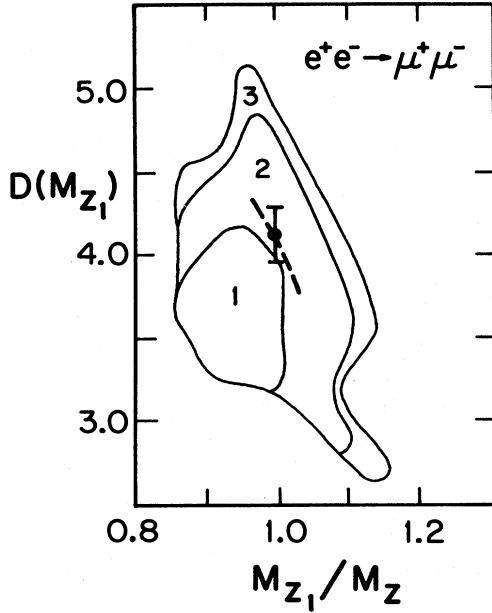


FIG. 3. Left-right-model predictions for the logarithmic derivative of the forward-backward asymmetry $D(\sqrt{s}) = s dA^{FB}/ds$ in $e^+e^- \rightarrow \mu^+\mu^-$ at $\sqrt{s} = M_{Z_1}$ versus M_{Z_1}/M_Z . Notation is as in Fig. 1.

with the functions H_i^q defined by

$$H_1^q(m, s) = \int_{-\ln\sqrt{s}/m}^{\ln\sqrt{s}/m} x_+ f_q^p(x_+, m^2) x_- f_q^{\bar{p}}(x_-, m^2) dy, \quad (38a)$$

$$H_2^q(m, s) = \int_{-\ln\sqrt{s}/m}^{\ln\sqrt{s}/m} \frac{x_+ f_q^p(x_+, m^2) x_- f_q^{\bar{p}}(x_-, m^2)}{(1 + e^{-2y})^3} dy. \quad (38b)$$

Figure 4 shows the allowed range of A^{FB} on the Z_1 based on the structure functions of Owens and Reya.³²

III. "STANDARD Z_1 " IN LEFT-RIGHT MODELS

One might well ask what is required to "prove" that the standard model is the unique description of electroweak interactions in a given energy range. At currently accessible energies standard-model predictions are in agreement with all experimental results, but there exists alternative gauge models which do equally well. For left-right models the constraints of low-energy experiments imply that the second weak scale M_{Z_2} is at least $1.6 M_{Z_1}$. In Sec. II we discussed the restrictions on weak-interaction parameters from cross sections and asymmetry measurements. However, these results are dominated by interactions of the Z_1 and are only mildly affected by the Z_2 . Since low-energy experiments still allow a wide range of left-right model solutions, one might suspect that the degrees of freedom associated with the Z_2 will not be severely restricted by measurements at $\sqrt{s} \sim 100$ GeV, and the lower limit on M_{Z_2} will not be significantly changed. In fact, there do exist solutions in which the Z_1 is indistinguishable from the standard-model Z boson and which yet allow a relatively-low-mass Z_2 , as we will show below.

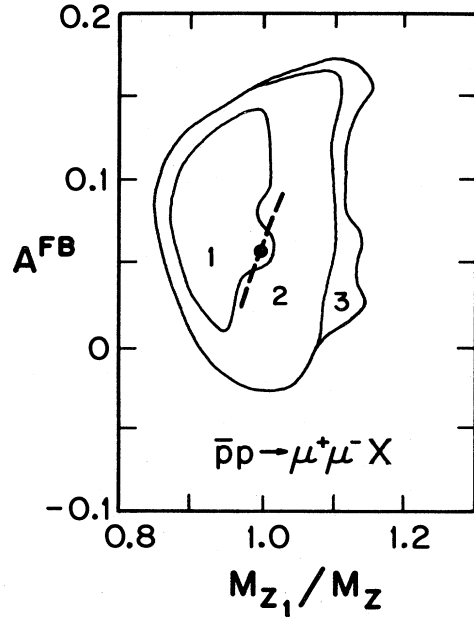


FIG. 4. Left-right-model predictions for the forward-backward asymmetry A^{FB} in $\bar{p}p \rightarrow \mu^+\mu^- X$. Notation as in Fig. 1.

A. Exact correspondence of Z_1 with the standard Z

The condition that the Z_1 in left-right models is exactly the same as the standard model Z in mass and fermion couplings (and hence width) corresponds to the constraints

$$\begin{aligned} \rho_1 &= 1, \\ x_L &= x_W, \\ \rho_2 &= \eta x_R / (1 - x_L), \\ \psi &= 0, \end{aligned} \quad (39)$$

where x_W is the single parameter of the standard model deduced from the Z mass. The Z -boson matrix is diagonal. The Z_2 decouples from the Z_1 but still interacts with fermions; see Eq. (12). The Z_2 mass is then given by

$$\begin{aligned} M_{Z_2} &= M_Z(\alpha + \beta)/\eta \\ &= M_Z(1 - x_L)x_L^{1/2}x_R^{-1/2}(1 - x_L - x_R)^{-1/2}/\eta \end{aligned} \quad (40)$$

and its fermion couplings are

$$\begin{aligned} g_{A2}^f &= x_L^{1/2}x_R^{-1/2}(1 - x_L - x_R)^{-1/2} \\ &\quad \times [(1 - x_L - x_R)^{1/2}I_3^f - x_R Q_f], \end{aligned} \quad (41a)$$

$$\begin{aligned} g_{V2}^f &= x_L^{1/2}x_R^{-1/2}(1 - x_L - x_R)^{-1/2} \\ &\quad \times [(1 - x_L - x_R)^{1/2}I_3^f]. \end{aligned} \quad (41b)$$

There remain two free parameters, which we take to be η and x_R . The region of η - x_R space still allowed by the low-energy data at the 1σ level is shown in Fig. 5, as determined from a two-parameter Monte Carlo fit. The constraints of Eq. (39) were imposed with $x_L = 0.233$.

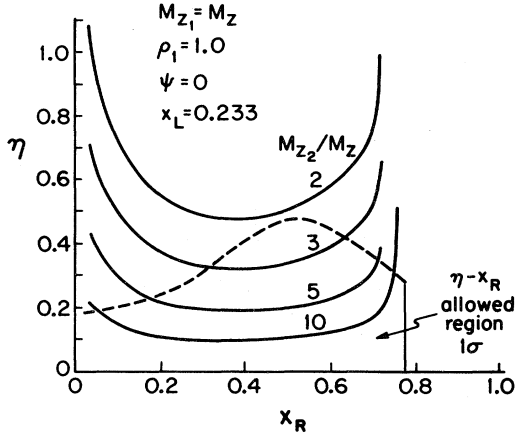


FIG. 5. Allowed region of the parameters η and x_R in a left-right model with a "standard" Z_1 coupling and mass ($M_{Z_1} = M_Z$ for $x_L = 0.233$). The dashed curve is the upper boundary of the allowed region. The contours represent M_{Z_2}/M_Z values.

Contours of the Z_2 mass, deduced from Eq. (40), are also given. The curves shift slightly for different values of x_L . In this scenario, a pure left-right-symmetric model ($x_L = x_R$) must have $M_{Z_2} \geq 4M_Z$, while the more general left-right-asymmetric model requires only that

$$M_{Z_2} \geq 2.2M_Z \approx 200 \text{ GeV}. \quad (42)$$

All measurements on the Z_1 will equal the standard values, but the energy dependence in the region of the Z_1 will be affected. The ranges of deviation from standard-model predictions off resonance when the Z_1 mimics the standard Z are shown in Table II. These deviations are much smaller than for the general left-right model and will probably not add any constraints in addition to those given by measurements on resonance unless significantly smaller experimental uncertainties are achieved than presently expected.

We next investigate the condition for a diagonal mass matrix in terms of Higgs vacuum expectation values. If the neutral Higgs scalars ϕ_i which obtain a nonzero vacuum expectation value v_i transform as (I_i, J_i, K_i) under $SU(2)_L \times SU(2)_R \times U(1)_{B-L}$, the off-diagonal entry in the Z mass matrix can be written

$$B = \sum_i I_i [\beta I_i + (\alpha + \beta) J_i] v_i^2. \quad (43)$$

TABLE II. Same as Table I for left-right models in which the Z_1 is identical in all respects to the standard Z of the same mass.

	Maximal left-right deviation $Z_1 \rightarrow Z$
A_{\min}^{FB}	+0.04
$M_{Z_1} - (s_{\min})^{1/2}$	$\pm 0.5 \text{ GeV}$
A_{\max}^{FB}	-0.11
$(s_{\max})^{1/2} - M_{Z_1}$	$\pm 1 \text{ GeV}$
$M_{Z_1} - (s_0)^{1/2}$	$\pm 0.1 \text{ GeV}$

The diagonal condition $B = 0$ is

$$x_R / (1 - x_L) = - \left[\frac{\sum_i I_i J_i v_i^2}{\sum_i I_i^2 v_i^2} \right] / \left[\frac{\sum_i I_i^2 v_i^2}{\sum_i I_i^2 v_i^2} \right]. \quad (44)$$

If $J_i = -I_i$ for all ϕ_i with nonzero I_i , then Eq. (44) is satisfied if x_R is equal to $1 - x_L$. However, the C boson would then be massless since no neutral Higgs boson can have $J_i = -I_i$ and also have nonzero K_i . For x_R less than but near $1 - x_L$, M_{Z_2} is very large and the model is indistinguishable from the standard model at observable energies.

Still another possibility would be to have all v_i which contribute to B be small compared to 100 GeV, but this forces A to be small also, in contradiction with Eq. (7a) with $\rho_1 = 1$.

The only consistent means of obtaining Eq. (44) exactly, which also allows a reasonably low Z_2 mass, is coincidental cancellation. This can happen for any value of x_R in its allowed range using conventional Higgs doublets and triplets assuming proper adjustment of vacuum expectation values. A somewhat wider range of parameters will be allowed since the exact constraints of Eq. (39) will not be realized in an actual experiment. From a Monte Carlo sampling of the parameters with the resonance measurements falling within the experimental uncertainties listed in Table II, we find that the parameter x_L is still constrained to be very close to x_W , but ρ_1^2 can be as low as 0.5 at the 1σ level. Such solutions will have ρ_2^2 near 0.5 so that $\rho_1^2 + \rho_2^2 \approx 1$ is satisfied. Thus, the tuning does not have to be precise. However, solutions with $M_{Z_2} < 3M_Z$ still require $\rho_1^2 \approx 1$. In this latter case, the $\eta - x_R$ allowed region and minimum M_{Z_2} contours are similar to the M_{Z_2} contours of Fig. 5.

B. Detecting the Z_2 in $\bar{p}p$

If the Z_1 boson of left-right models is indistinguishable from the standard-model Z , then the Z_2 must be detected directly. The cross section for $\bar{p}p \rightarrow \mu^+ \mu^- X$ is given in Eq. (34). Integrating over a resonant peak gives

$$\sigma_{\text{peak}}^{q\bar{q}} = 6\pi^2 \Gamma_{Z_i} (B_q^i / 3) B_\mu^i / M_{Z_i}^2, \quad (45)$$

where B_f^i is the branching ratio for $Z_i \rightarrow f\bar{f}$. After folding in the structure functions and integrating over y , the resonant $\bar{p}p$ cross section becomes

$$\sigma_{\text{peak}} = \frac{4\pi^2}{3} \frac{\Gamma_{Z_i}}{M_{Z_i}^3} B_\mu^i \sum_q B_q^i H^q, \quad (46)$$

where H^q is defined in Eq. (38) and the sum is over all quark and antiquark flavors in the proton.

The branching ratios for the Z_2 when the Z_1 is identical to the standard Z are

$$B(Z_2 \rightarrow f\bar{f}) = c_f \frac{[1 + (1 - 4|Q_f^f|)r]^2 + [1 - r]^2}{16[3(1 - r)^2 + 2r^2]}, \quad (47)$$

with color factors $c_f = 3$ for quarks and $c_f = 1$ for leptons of charge Q_f . The quantity r is defined as $r = x_R /$

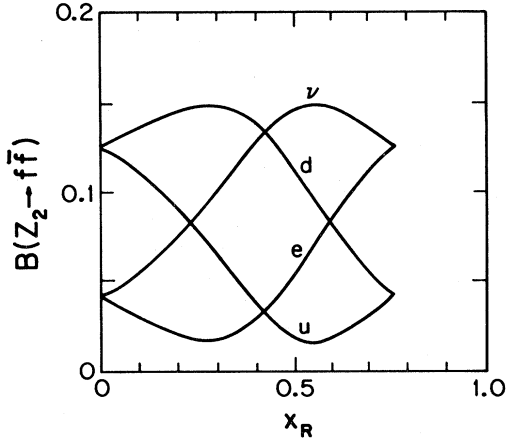


FIG. 6. Branching ratios for the Z_2 versus x_R in left-right models with a “standard” Z_1 , defined as in Fig. 5.

$(1-x_L)$. The Z widths simplify to

$$\Gamma_{Z_2} = \frac{\sqrt{2}}{3\pi} G_F M_{Z_1}^2 M_{Z_2} [3(1-x_L-x_R)^2 + 2x_R^2], \quad (48a)$$

$$\Gamma_{Z_1} = \frac{\sqrt{2}}{3\pi} G_F M_{Z_1}^3 [3-6x_L+3x_L^2], \quad (48b)$$

when fermion masses are negligible. Figure 6 shows the branching ratios versus x_R for $x_L=0.233$. Small changes in the value of x_L will shift these results only slightly. From Fig. 5 we see that $x_R \approx 0.3-0.6$ is needed for $M_{Z_2} < 3M_{Z_1}$. Grand unified left-right models require $x_R \geq x_L \approx 0.23$. However, for this range of x_R the u -quark branching ratio for the Z_2 is lower than for the Z_1 [$B(Z_1 \rightarrow \bar{u}u) \approx 0.11$, $B(Z_1 \rightarrow \bar{d}d) \approx 0.14$], so that Z_2 production is suppressed in $\bar{p}p$ colliders.¹²

Table III lists the σ_{peak} for dimuon mass values of $M_{Z_1}=90$ GeV and $M_{Z_2}=200$ GeV at $\sqrt{s}=540$ and 2000 GeV. At each energy the Z_1 entry corresponds to the standard-model prediction. The low-lying Z_2 may just be detectable in a $\bar{p}p$ experiment with integrated luminosity of 1 pb^{-1} at $\sqrt{s}=2000$ GeV. The cross section falls off rapidly for higher values of M_{Z_2} . Figure 7 shows $d\sigma/dm$ for the case $M_{Z_2}=200$ GeV and $x_R=0.5$.

IV. DISCUSSION OF DATA ANALYSIS

In the preceding sections, the allowed regions of parameters were determined by a least squares fit to neutral-current data similar to that performed in Ref. 3, except

TABLE III. Integrated cross section for $\bar{p}p \rightarrow \mu^+\mu^-X$ at a Z resonance in left-right models in which the Z_1 is identical to the standard Z for the case $Z_1=90$ GeV, $Z_2=200$ GeV.

	m (GeV)	\sqrt{s} (GeV)	σ_{peak} (pb)
Z_1	90	540	30
Z_2	200	540	0.076
Z_1	90	2000	300
Z_2	200	2000	4.5

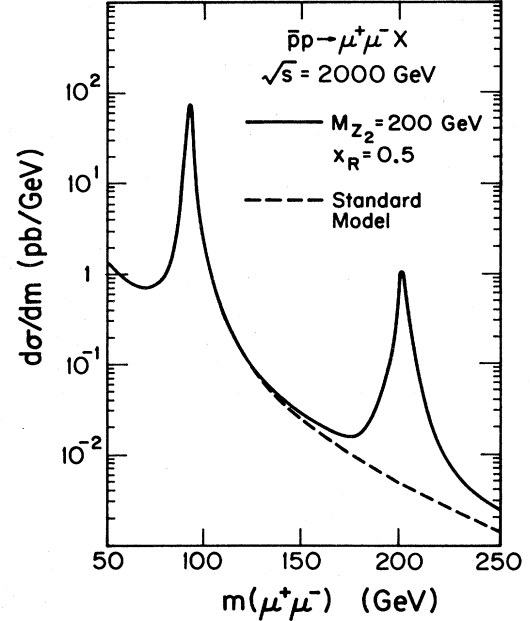


FIG. 7. Prediction for the cross section $d\sigma/dm$ versus dimuon mass m for the Drell-Yan process $\bar{p}p \rightarrow \mu^+\mu^-X$ at $\sqrt{s}=2000$ GeV when the Z_1 boson is identical to the standard Z . The case shown corresponds to $M_{Z_2}=200$ GeV and $x_R=0.5$.

that new measurements of $e^+e^- \rightarrow l^+l^-$ and atomic parity violation were used in place of the corresponding earlier data. The recent results from PETRA on $e^+e^- \rightarrow e^+e^-$ and $e^+e^- \rightarrow \mu^+\mu^-$ give the constraints³³

$$4g_V^2 = -0.04 \pm 0.06, \quad (51a)$$

$$4g_A^2 = 0.26 \pm 0.07, \quad (51b)$$

where g_V and g_A are the effective vector and axial-vector couplings for charged leptons in the low-energy Hamiltonian. We have chosen the normalization in Eq. (51) consistent with Eq. (11). The new measurement of atomic parity violation in cesium yields²⁴

$$Q_W^{\text{Cs}} = -55.1 \pm 9.07 \pm 4.5 \pm 5.5. \quad (52)$$

The first two errors are statistical and systematic errors in the experiment; the last is the uncertainty of the atomic-theory calculation. Left-right models predict

$$Q_W^{\text{Cs}}(\text{th}) = -(\rho_1^2 + \rho_2^2 - \rho_2\eta)(20 + 220x_L) + (\eta^2 - \rho_2\eta)(20 + 220x_R). \quad (53)$$

For the standard model with $x_L=0.233$ the theoretical value is $Q_W^{\text{Cs}}(\text{th})=71.3$.

The data on e^+e^- annihilation do not provide a severe constraint on the parameters of left-right models. However, the lower limit allowed for the Z_2 mass in left-right models depends sensitively on the atomic parity-violation data. Our Monte Carlo analysis shows that left-right models with a low Z_2 mass generally have $\eta \sim 0.5$, $\rho_2 \leq 0.1$, and $\rho_1 \sim 1$. We see from Eq. (53) that these parameter values decrease the magnitude of $Q_W^{\text{Cs}}(\text{th})$ from the standard-model prediction. Previous measurements³⁴ in-

indicated a larger $|Q_W|$ than the theoretical prediction of the standard model, whereas the new data indicates a smaller value. Thus, the old data was restrictive for low M_{Z_2} solutions; the limit obtained was $M_{Z_2} \gtrsim 2M_{Z_1}$ at the 1σ level for a five-parameter fit. When the neutral-current analysis is carried out with the new atomic parity-violation data, we find the less severe constraint

$$M_{Z_2} \gtrsim 1.6M_{Z_1} \simeq 150 \text{ GeV} (1\sigma). \quad (54)$$

V. SUMMARY

In this paper we have compared the high-energy predictions of a general left-right model in fermion-antifermion annihilation experiments with those of the standard model to determine how well they might be distinguished by measurements in the region of the standard Z boson resonance. We find that only those parameters which contribute to the Z_1 mass and fermion couplings are well determined, as the Z_1 dominates the behavior in that energy region. On the Z_1 resonance, where the most precise measurements will occur, nothing can be learned about parameters relating only to the Z_2 . In principle, off-resonance behavior contains some information on the undetermined parameters, but the effects are of the order of a few percent or less, which may not be observable given the anticipated experimental uncertainties. The largest nonstandard predictions at energies near the Z_1 mass occur above reso-

nance where severe radiative corrections may obscure the effect.

Our conclusion is that parameters in a left-right model associated only with the Z_2 will not be greatly constrained at energies below 120 GeV. In fact, there exists a class of left-right models in which the Z_1 is identical to the standard Z in all respects, but allows the Z_2 as low as 200 GeV. The lower bound on M_{Z_2} comes predominantly from the atomic parity-violation measurement and would not be raised significantly by measurements at energies in the region of the Z_1 mass unless they are very accurate. The identity of the Z_1 with the standard model Z is possible in a left-right model with doublet and triplet Higgs representations. In such a model production of the Z_2 with a mass near 200 GeV may be possible in a $\bar{p}p$ experiment at $\sqrt{s} = 2000$ GeV with integrated luminosity of at least 1 pb^{-1} .

ACKNOWLEDGMENTS

This research was supported in part by the University of Wisconsin Research Committee with funds granted by the Wisconsin Alumni Research Foundation, in part by the U. S. Department of Energy under contracts DE-AC02-76ER00881, DE-AM03-76SF00235, and W-7405-Eng-82, and in part by the Office of Basic Science (KA-01-01), Division of High Energy Physics and Nuclear Physics.

- ¹S. Weinberg, Phys. Rev. Lett. **19**, 1264 (1967); A. Salam and J. C. Ward, Phys. Lett. **13**, 168 (1964); S. L. Glashow, Nucl. Phys. **22**, 579 (1961); S. L. Glashow, J. Iliopoulos, and L. Maiani, Phys. Rev. D **2**, 1285 (1970).
- ²See, for example, F. W. Büsser, in *Neutrino 81*, proceedings of the 1981 International Conference on Neutrino Physics and Astrophysics, Hawaii, edited by R. J. Cence, E. Ma, and A. Roberts (University of Hawaii High Energy Physics Group, Honolulu, 1981), Vol. II, p. 351.
- ³V. Barger, Ernest Ma, and K. Whisnant, Phys. Rev. D **26**, 2378 (1982).
- ⁴J. C. Pati and A. Salam, Phys. Rev. D **10**, 275 (1974); R. N. Mohapatra and J. C. Pati, *ibid.* **11**, 566 (1975); **11**, 2558 (1975); G. Senjanović and R. N. Mohapatra, *ibid.* **12**, 1502 (1975); H. Fritzsch and P. Minkowski, Nucl. Phys. **B103**, 61 (1976); E. Ma, *ibid.* **B121**, 421 (1977).
- ⁵M. A. B. Bég, R. V. Budny, R. Mohapatra, and A. Sirlin, Phys. Rev. Lett. **38**, 1252 (1977).
- ⁶I. Liedtke, J. Maalampi, and M. Roos, Nucl. Phys. **B146**, 157 (1978).
- ⁷R. E. Marshak and R. N. Mohapatra, Phys. Lett. **91B**, 222 (1980).
- ⁸T. G. Rizzo and G. Senjanović, Phys. Rev. Lett. **46**, 1315 (1981); Phys. Rev. D **24**, 704 (1981).
- ⁹X. Li and R. E. Marshak, Phys. Rev. D **25**, 1886 (1982).
- ¹⁰N. G. Deshpande and D. Iskandar, Phys. Lett. **87B**, 383 (1979); Nucl. Phys. **B167**, 223 (1980).
- ¹¹S. Rajpoot, Phys. Lett. **108B**, 303 (1982).
- ¹²R. W. Robinett and J. L. Rosner, Phys. Rev. **D 25**, 3036 (1982).
- ¹³M. K. Parida and A. Raychaudhuri, Phys. Rev. D **26**, 2364 (1982).
- ¹⁴G. Fogleman and T. G. Rizzo, Phys. Lett. **113B**, 240 (1982).
- ¹⁵N. G. Deshpande and R. J. Johnson, Phys. Rev. D **27**, 1165 (1983).
- ¹⁶H. Georgi and S. Weinberg, Phys. Rev. D **17**, 275 (1978).
- ¹⁷E. H. de Groot, G. J. Gounaris, and D. Schildknecht, Phys. Lett. **85B**, 399 (1979); **90B**, 427 (1980); Z. Phys. C **5**, 127 (1980).
- ¹⁸V. Barger, W. Y. Keung, and E. Ma, Phys. Rev. Lett. **44**, 1169 (1980); Phys. Rev. D **22**, 727 (1980); Phys. Lett. **94B**, 377 (1980).
- ¹⁹E. H. de Groot and D. Schildknecht, Phys. Lett. **95B**, 128 (1980); Z. Phys. C **10**, 55 (1981); **10**, 139 (1981).
- ²⁰V. Barger, E. Ma, and K. Whisnant, Phys. Rev. Lett. **46**, 1501 (1981); Phys. Rev. D **25**, 1384 (1982).
- ²¹V. Barger, E. Ma, and K. Whisnant, Phys. Lett. **107B**, 95 (1981).
- ²²V. Barger, K. Whisnant, and W. Y. Keung, Phys. Rev. D **25**, 291 (1982).
- ²³J. E. Kim, P. Langacker, M. Levine, and H. H. Williams, Rev. Mod. Phys. **53**, 211 (1981).
- ²⁴M. A. Bouchiat, J. Guena, L. Hunter, and L. Pottier, Phys. Lett. **117B**, 358 (1982).
- ²⁵W. Hollik, Z. Phys. C **8**, 149 (1981); W. B. Lindquist, in *Proceedings of the Z⁰ Physics Workshop, Ithaca, New York, 1981*, edited by M. E. Peskin and S.-H.H. Tye (Laboratory of Nuclear Studies, Cornell University, Ithaca, 1981), p. 116.
- ²⁶J. Ellis and M. K. Gaillard, in *Physics with High Energy e⁺e⁻ Collider Beams* (CERN Report No. 76-18, 1976), p. 21.

- ²⁷*Proceedings of the SLAC Workshop on Experimental Use of the SLAC Linear Collider*, edited by J. Dorfan and G. Trilling (SLAC Report No. 247, 1982), p. 115.
- ²⁸M. Greco, G. Pancheri-Srivastava, and Y. Srivastava, Nucl. Phys. **B171**, 118 (1980).
- ²⁹W. J. Marciano and A. Sirlin, in *Proceedings of Second Workshop on Grand Unification*, Ann Arbor, Michigan, 1981, edited by J. P. Leveille, L. R. Sulak, and D. G. Unger (Birkhauser, Boston, 1981), p. 151.
- ³⁰W. J. Marciano and Z. Parsa, in *Proceedings of the Z⁰ Physics Workshop* (Ref. 25), p. 127.
- ³¹G. Barbiellini, B. Richter, and J. L. Siegrist, Phys. Lett. **106B**, 414 (1981); K. J. F. Gaemers, R. Gastmans, and F. M. Renard, Phys. Rev. D **19**, 1605 (1978); E. Ma and J. Okada, Phys. Rev. Lett. **41**, 287 (1978).
- ³²J. F. Owens and E. Reya, Phys. Rev. D **17**, 3003 (1978).
- ³³TASSO collaboration results reported by D. Luke, XXIst International Conference on High Energy Physics, Paris, 1982 (unpublished).
- ³⁴L. M. Barkov and M. S. Zolotarev, Phys. Lett. **85B**, 308 (1979); P. Bucksbaum, E. Commins, and L. Hunter, Phys. Rev. Lett. **46**, 640 (1981); J. H. Hollister *et al.*, *ibid.* **46**, 643 (1981).